Chemistry & Biology
Article

Recognition of Intermediate Functionality by Acyl Carrier Protein over a Complete Cycle of Fatty Acid Biosynthesis

Eliza Płoskoń,[1] Christopher J. Arthur,[1] Amelia L.P. Kanari,[1] Pakorn Wattana-amorn,[1] Christopher Williams,[1] John Crosby,[1] Thomas J. Simpson,[1] Christine L. Willis,[1] and Matthew P. Crump[1,*]
[1]School of Chemistry, University of Bristol, Cantock's Close, Bristol BS8 1TS, United Kingdom
*Correspondence: matt.crump@bristol.ac.uk
DOI 10.1016/j.chembiol.2010.05.024

SUMMARY

It remains unclear whether in a bacterial fatty acid synthase (FAS) acyl chain transfer is a programmed or diffusion controlled and random action. Acyl carrier protein (ACP), which delivers all intermediates and interacts with all synthase enzymes, is the key player in this process. High-resolution structures of intermediates covalently bound to an ACP representing each step in fatty acid biosynthesis have been solved by solution NMR. These include hexanoyl-, 3-oxooctanyl-, 3*R*-hydroxyoctanoyl-, 2-octenoyl-, and octanoyl-ACP from *Streptomyces coelicolor* FAS. The high-resolution structures reveal that the ACP adopts a unique conformation for each intermediate driven by changes in the internal fatty acid binding pocket. The binding of each intermediate shows conserved structural features that may ensure effective molecular recognition over subsequent rounds of fatty acid biosynthesis.

INTRODUCTION

Essential for all organisms, fatty acid synthases (FASs) catalyze the biosynthesis of fatty acids via an iterative process whereby the carbon chain is successively elongated by condensation with malonate. The resultant β-keto thiol ester is further converted by a sequence of ketoreduction, dehydration, and enoyl reduction to the fully saturated acyl thiol ester in a subsequent elongation cycle (Figure 1A). Bacterial FASs are composed of discrete proteins (type II), while in mammals and fungi all of the FAS enzymatic activities are placed on a single polypeptide that associate to form large megasynthases (type I) (White et al., 2005). In both classes, the nascent fatty acids are shuttled between each catalytic activity via an acyl carrier protein (ACP). These intermediates are covalently bound as thiol esters to a phosphopantetheine cofactor (4′-PP) that is attached to a conserved serine on the ACP (Byers and Gong, 2007).

The FAS enzymes must catalyze a series of reactions in a specific sequence within one biosynthetic cycle, but it is unknown whether ACP is controlled or directed to associate and dissociate with each component in that order. In the type I mammalian FAS, biosynthesis may be directed by adjusting the conformation of the megasynthase and consequently changing the positions of catalytic domains in relation to the ACP (Brignole et al., 2009). This in turn might enable division of the β-carbon processing and substrate loading phases from the condensation steps. This structural and dynamic control may permit certain mechanistic simplifications that enable more efficient fatty acid production, such as the lack of the energetically costly sequestration of saturated acyl chains within the hydrophobic core of the ACP (Płoskoń et al., 2008).

Bacterial FASs do not display such an arrangement and at present the structure of any higher order noncovalent type II complex is unknown. This system may therefore possess other means of controlling and directing fatty acid production. It has been speculated that conformational changes in the carrier protein in response to the length and, possibly, the functionality present on the acyl chain may modulate these protein-protein interactions (Roujeinikova et al., 2007). In this case, for recognition to take place, there must be distinguishable changes in the acyl-ACP after each modification. Alternatively, there may be little recognition and fatty acid modification may take place through a series of random associations. In this case, an incorrect enzyme-ACP encounter would simply lead to a nonproductive complex followed by dissociation.

ACP structural studies to date have only focused on the interactions with fully saturated acyl chains that are easily prepared (Roujeinikova et al., 2007; Zornetzer et al., 2006). Solution NMR and crystal structures of acylated FAS ACPs show that the aliphatic portion of the fatty acid is buried within the hydrophobic core of the ACP four helix bundle. This results in a conformational change in the third helix (Upadhyay et al., 2009; Wu et al., 2009) that may contribute to enzyme recognition. NMR and molecular dynamic studies of *Escherichia coli* apo, holo-, and acyl-ACPs (Chan et al., 2008; Kim et al., 2006) and 3-hydroxydecanoyl-ACP from *Plasmodium falciparum* have also suggested helix III and the preceding loop play a role in recognition of synthase partners (Colizzi et al., 2008). Some structural details of ACP conformational adjustment in response to increased saturated acyl chain length have therefore been revealed. There is no information, however, about the molecular recognition of unsaturated intermediates by ACP and any related conformational changes that might occur during the remainder of the biosynthetic cycle.

To begin to address this question, we have solved the solution NMR structures of a representative set of acyl FAS ACPs from

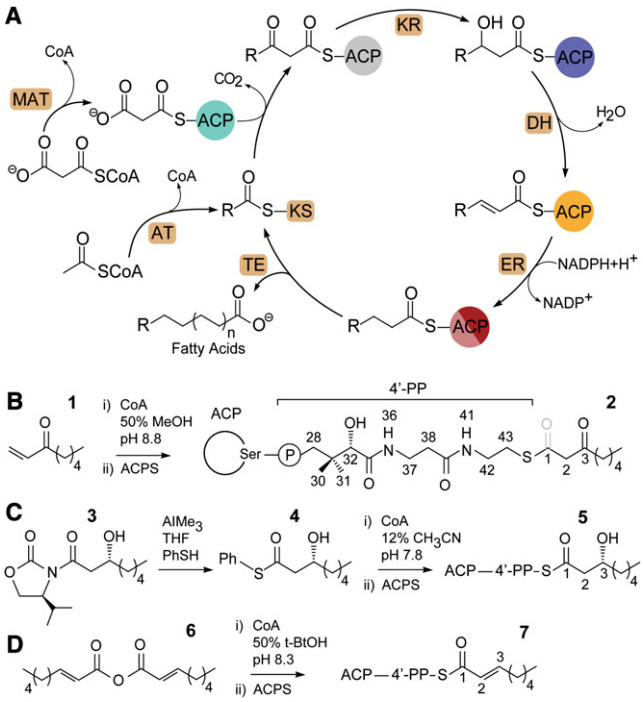

Figure 1. Generalized Scheme of the FAS Catalytic Cycle

(A) The reaction is initiated by the transfer of the acyl moiety to the ketosynthase, catalyzed by the acetyl-CoA-ACP transacylase (AT) and the malonyl moiety to ACP catalyzed by malonyl-CoA-ACP transacylase (MAT). The ketosynthase (KS) catalyzes the decarboxylative condensation of the acyl intermediate with malonyl-ACP to yield the 3-oxoacyl-ACP. This reaction is followed by reduction of the β-keto group by the ketoreductase (KR). The resulting 3-hydroxyacyl-ACP is dehydrated by a dehydratase (DH) to 2-enoyl-ACP, which is reduced by the enoylreductase (ER) to the fully saturated acyl substrate for further cyclic elongation. The reaction proceeds until the desired chain length is produced, which is than released from the ACP by the thioesterase (TE).

(B) Synthetic summary for 3-oxooctanyl-ACP, (C) 3*R*-hydroxyoctanoyl-ACP, and (D) 2-octenoyl-ACP. The numbering indicated for 4′-PP group is used in the text.

Streptomyces coelicolor for one complete fatty acid biosynthetic cycle that include hexanoyl, 3-oxooctanyl, 3*R*-hydroxyoctanoyl, 2-octenoyl ,and octanoyl derivatives. To enable these studies, a series of modified CoA thiol esters of functionalized biosynthetic intermediates were chemically synthesized and enzymatically attached to the ACP. Herein it is shown that all acyl intermediates are sequestered into the hydrophobic cavity of the ACP to varying extents, and that the cavity enlarges with an increase in the length of the acyl chain from six to eight carbon atoms. Most significantly, we report changes in carrier protein conformation that occur in response to the functionality on the bound acyl intermediate.

RESULTS

Sample Preparation

Samples of $^{13}C/^{15}N$-labeled FAS ACP were prepared as reported previously and derivatized using the relaxed specificity of *S. coelicolor* holo ACP synthase (ACPS) for modified coenzyme As (CoA) (the 4′-PP group is derived from CoA in the wild-type reaction) (Cox et al., 1997). In our representative round of fatty acid biosynthesis (hexanoyl to octanoyl), the first reaction is the KS catalyzed condensation of malonyl-ACP with a hexanoyl group to yield 3-oxooctanoyl-ACP. The holo and fully reduced hexanoyl-ACP (and octanoyl-ACP for the end of the cycle) were prepared from their respective, commercially available acyl-CoAs. Attempts, however, to synthesize 3-oxooctanoyl-CoA or to modify ACP with acetoacetal-CoA were unsuccessful. The time the ACP and the respective CoA were kept in the reaction buffer (pH 8.8) was limited to only 1 hr (after which the pH was decreased to 7.0). Despite this precaution, rapid hydrolysis of the oxoacyl group from the ACP yielded 100% holo ACP. Lowering the pH of the phosphopantetheinylation reaction was tested but was found to give poor conversion of the ACP. To overcome this problem, we have recently demonstrated the use of stable 3-oxo thioether derivatives as mimics of keto-acyl groups (Evans et al., 2009). Hence, the revised target was 3-oxooctanyl-CoA, which retains the C_3 ketonic carbonyl group (C_3 = O) but lacks the C_1 carbonyl (C_1 = O), as a mimic of 3-oxooctanoyl-CoA. 3-oxooctanyl-CoA was prepared via Michael addition of CoA to oct-1-en-3-one (Figure 1B, **1**) and then transferred to ^{13}C, ^{15}N FAS apo ACP using ACPS (Figure 1B, **2**). Efficient transfer of the acyl phosphopantetheine chain was achieved by incubating the ACP with a catalytic amount of ACPS and a 5-fold molar excess of the relevant CoA derivative. The transfer was shown to be complete within 1 hr by mass spectrometry.

In the second step of fatty acid biosynthesis, KR catalyzed ketoreduction of 3-oxooctanoyl-ACP would then yield 3*R*-hydroxyoctanoyl-ACP. 3*R*-hydroxyoctanoyl-CoA was prepared by transesterification of S-phenyl 3*R*-hydroxyoctanethioate (see Supplemental Experimental Procedures available online) with free CoA (Figure 1C, **4, 5**) using the method of Jia and Stubbe (Jia et al., 2001).

In the third step of fatty acid biosynthesis, 2-octenoyl-ACP (Figure 1D, **7**) was formed by the dehydration of 3*R*-hydroxyoctanoyl-ACP catalyzed by the DH. 2-octenoyl-CoA was synthesized using the procedure of Rasmussen and Knudsen (Figure 1D; Rasmussen et al., 1990).

Initial analysis of Acyl Chain Binding

The ^{1}H-^{15}N HSQC spectrum of *S. coelicolor* FAS ACP shows excellent chemical shift dispersion that allows changes in the local environment of amide resonances to be followed (Arthur et al., 2009). ^{1}H-^{15}N HSQC spectra were recorded under identical buffer and temperature conditions (pH 7.0, 25°C) for hexanoyl-, 3-oxooctanyl-, 3*R*-hydroxyoctanoyl-, 2-octenoyl-, and octanoyl-ACPs. Chemical shift values were compared by calculating average shift differences δΔ between the spectra for adjacent steps in the fatty acid cycle (i.e., hexanoyl- to 3-oxooctanyl-ACP) (Figure 2) (Pellecchia et al., 1999). HSQC spectra of the apo and holo forms were also acquired under the same conditions as the acyl-ACP forms (see Figure S1). Upon attachment of the phosphopantetheine group only residues surrounding the attachment site (S40) are affected suggesting that the apo and holo forms show very similar conformations although minor side-chain rearrangements cannot be ruled out as previously observed for the actinorhodin ACP from *S. coelicolor* (Evans et al., 2008).

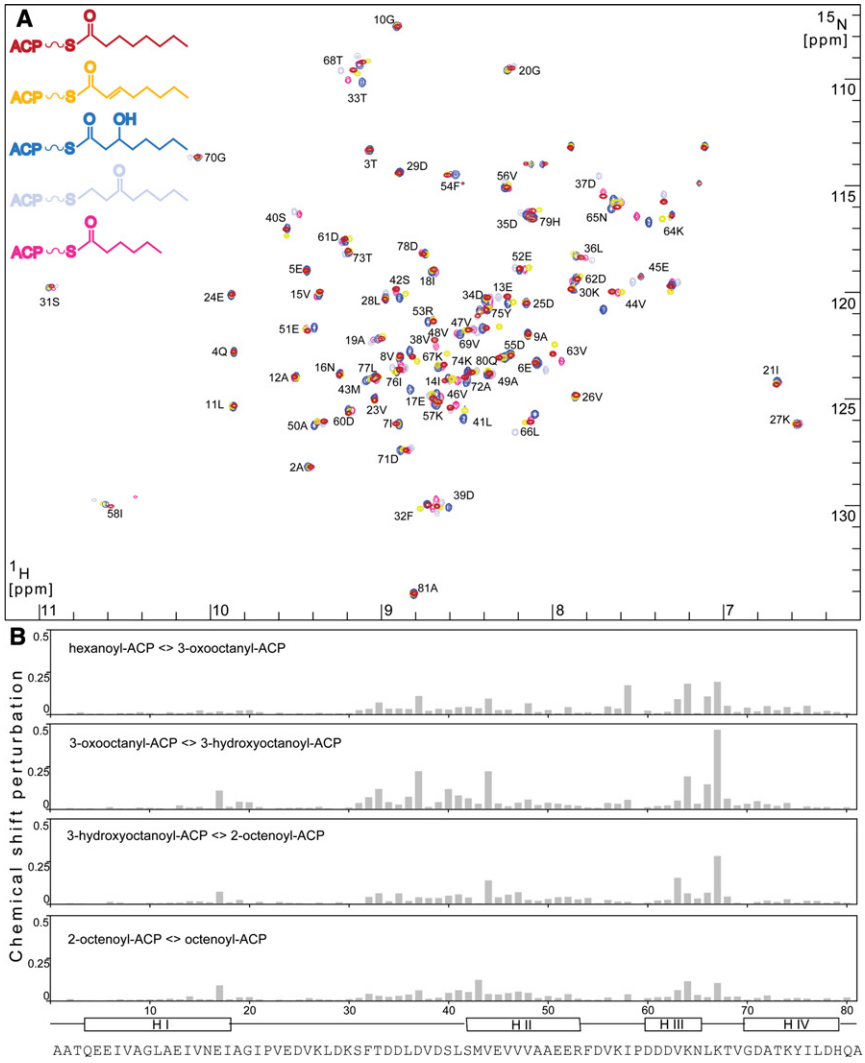

Figure 2. Comparison of the ^{1}H-^{15}N HSQC Spectra of the Derivatized ACPs

(A) Superimposed ^{1}H-^{15}N HSQC spectra of uniformly ^{15}N-labeled forms of *S. coelicolor* ACP. Shown are hexanoyl-ACP (pink), 3-oxooctanyl-ACP (gray), 3*R*-hydroxyoctanoyl-ACP (blue), 2-octenoyl-ACP (yellow), and octanoyl-ACP (red).

(B) Chemical shift perturbations ($\delta\Delta_{av}$) versus holo ACP plotted against residue number. The primary sequence of *S. coelicolor* FAS ACP and the positions of the α-helices are indicated. See also Figure S1.

tures of this representative set of acyl ACPs. Chemical shifts were unambiguously assigned using standard multidimensional multinuclear NMR experiments. Triple resonance data were not acquired for 3*R*-hydroxyoctanoyl-ACP that could be assigned manually on the basis of similarity to other structures. For the others, a full set of triple resonance experiments was acquired. Nuclear Overhauser effect (NOE) constraints were assigned semiautomatically using the Ambiguous Restraints for Iterative Assignment (ARIA) algorithm (Nilges et al., 1997). As the acyl-phosphopantetheine groups of the ACPs have been added in vitro, they are not isotopically labeled. This feature enabled us to distinguish NOEs originating from the interaction of the ^{12}C/^{14}N labeled phosphopantetheine and the ^{13}C/^{15}N labeled protein using 2D filtered experiments (Peterson et al., 2004). Protein-ligand and intra-ligand NOE distance restraints from 2D F_2f- and F_1f-F_2f NOESY experiments were assigned manually.

Although the respective CoAs were stable, for 3*R*-hydroxyoctanoyl-ACP formation of the dehydrated, enoyl form, was observed to steadily occur over time (up to 25% after 24 hr). Likewise, a population of 3*R*-hydroxyoctanoyl-ACP was observed in the 2-octenoyl-ACP spectra (up to 20% after 5 days). The NOESY spectrum of a fresh sample of octenoyl-ACP, however, only showed peaks from octenoyl-ACP. For the 3*R*-hydroxyoctanoyl-ACP sample, therefore, CN-NOESY and 2D-F_2f-NOESY experiments were acquired on two separate samples. These experiments were sufficient to fully assign both protein and acyl-phosphopantetheine resonances. CN-NOESY data for this sample were acquired over 24 hr (normally 96 hr) and the filtered experiment was recorded over 7 hr (normally 24 hr). The experiment times were changed in order to limit the contribution of the enoyl form in the acquired spectra. However, there was still the potential for a minor contribution to a NOESY peak from the octenoyl-ACP. Therefore, we used the clean spectrum of octenoyl-ACP to determine whether there were contributions to peaks in the 3*R*-hydroxyoctanoyl ACP (i.e., where chemical shifts

Over this complete cycle of fatty acid biosynthesis, elongation of the chain from six to eight carbon atoms results in chemical shift perturbations for residues S40, M43, V48, I58, and K64 in helix II and III. Additionally, two residues on loop 1 (F32, T33) and residues 10–20 in helix I are visibly perturbed, but to a lesser degree. Such changes were not unexpected given the well-characterized binding behavior of fully saturated acyl chains (Upadhyay et al., 2009). However superposition of the ^{1}H-^{15}N HSQC spectra of the intervening fatty acid cycle intermediates revealed that each derivatized ACP displayed a distinct pattern of chemical shift perturbations (Figures 2B–2E). Again, these were found principally in regions surrounding helix II and III and loop 1 but varied in their sign change and magnitude. This indicated sequestration of each intermediate perhaps with subtle modulation of the binding mode depending on the exact functionality of the acyl intermediate.

Three-Dimensional Structures of the Derivatized ACPs

Following our initial HSQC-based study, it was clear that to fully understand the nature of chain sequestration during the fatty acid biosynthetic cycle it would be necessary to solve the struc-

were degenerate) and add corrections to the restraints used. It is important to stress, however, that in the critical regions of the structure that interact with the acyl chain, the majority of resonances were distinguishable between the two forms. For other peaks that were indistinguishable between the two forms, and were located on parts of the structure that did not change, the sizeable correction added to a NOE constraint used in the calculation would more than compensate for any small differences in the peak intensity. The total number of NOE peaks identified in both the CN-NOESY and 2D-F_2f-NOESY (3156) was sufficient to elucidate the 3*R*-hydroxyoctanoyl-ACP structure to high resolution.

We were therefore able to solve solution structures of hexanoyl-, 3-oxooctanyl-, 3*R*-hydroxyoctanoyl-, 2-octenoyl-, and octanoyl-ACP to high resolution and precision. The structural statistics for all ensembles are summarized in Table 1 and a comparison of the percentage number of NOEs that are long range on a per residue basis for all five structures is given in Figure S2. All of the derivatized ACP structures are well defined by the NMR data with low root mean square deviations (RMSDs) for the ensembles of structures (20 models each) over the backbone and side-chain atoms in the helices. More mobile regions including the loop regions and N terminus lead to a higher RMSD when all atoms are included. Octanoyl-ACP shows a marginally higher RMSD for the ensemble although this is still well defined at 0.42 Å over the secondary structure elements. The reason for the higher RMSD is due to the lower overall number of NOEs due to an inferior CN-NOESY spectrum for this sample. The distribution of long-range NOEs, however, is broadly similar for all five structures and therefore, despite fewer NOEs, the impact on the octanoyl-ACP structure was minimal. This structure utilizes a sizeable number of NOEs (1952) which is comparable or greater than related studies. In the acylated spinach ACP structures, for example, high-resolution structures were determined using 1600–1700 NOE restraints (Zornetzer et al., 2006) or 1062 NOE restraints in the *E. coli* butyryl ACP structure (Wu et al., 2009).

Consistent with known ACP structures, the derivatized ACPs adopt a four helical bundle (Figures 3A–3E). Helix I (residues Q4–I18) precedes the longest loop in the protein and in all structures is well defined. Helix II (residues S42–R53) contains conserved acidic residues (E48, E51) that have been suggested to belong to the ACP recognition motif (Zhang et al., 2003a, 2003b). Helices II and III are connected by loop 2. This begins with a conserved residue, F54, which plays an important role in stabilizing the protein core (Arthur et al., 2006; Flaman et al., 2001). Helix III is the shortest in the protein and stretches from D60 to N65, while helix IV runs from G70 to H79. In all structures, the protein sequesters the acyl chain into the hydrophobic core between helices II and IV.

The opening to the acyl binding pocket is surrounded by the polar residue T33, the hydrophobe L41, and the charged residues, D60 and K64. The alkyl chain pocket (Figure 4) is lined by the side chains of residues: L11, F32, M43, V46, V47, A50, I58, V63, L66, A72, and I76 and the backbone of K67. F32 is conserved in type II FAS ACPs and this residue contributes to the surface of the binding pocket in all of the structures. The presence of this aromatic residue might have important implications for the ability of ACP to bind acyl chains, as this residue is not conserved in type I FAS ACPs. The phosphopantetheine chain is placed into a groove between helix II, III and loop 1 with the majority of it being solvent exposed. The number of NOE constraints between the protein and phosphopantetheine protons varies between structures with on average 5% of the total number (Table S1). This exceeds that reported in other NMR studies of acyl ACPs (Evans et al., 2009; Zornetzer et al., 2006).

Table 1. Summary of Structural Statistics for Ensembles of Hexanoyl-ACP (hex), 3-Oxooctanyl-ACP (3-oxooct), 3*R*-Hydroxyoctanoyl-ACP (3-OH-oct), 2-Octenyl-ACP (2-octen), and Octanoyl-ACP (oct)

	hex	*3-oxooct*	*3-OH-oct*	*2-octen*	*oct*
NOE restraints					
Intraresidue	942	927	644	785	643
Short range	994	969	784	662	459
Medium range	866	837	602	503	278
Long range	1755	1813	1126	912	579
Ambiguous	2094	2092	1018	722	464
Unambiguous	2464	2453	2138	2140	1495
Total	4558	4545	3156	2862	1959
TALOS restraints	41	40	39	39	42
Ramachandran plot statistics					
Most favored	80.6	82.3	82.3	80.6	84.8
Additional allowed	15.8	13.5	14.3	17.8	14.4
Generously allowed	2.6	3.5	2.7	1.6	0.8
Disallowed	1.0	0.7	0.7	0.0	0.0
RMSDs of the ensembles					
Backbone atoms in 2° structure[a]	0.21	0.26	0.31	0.33	0.42
Heavy atoms in 2° structure[a]	0.55	0.69	0.65	0.73	0.87
Backbone all residues	0.33	0.34	0.44	0.48	0.60
Heavy all residues	0.70	0.72	0.87	0.85	1.03
Violations within the ensemble					
NOE >0.3 Å	0.1	0.1	0	0	0.05
TALOS >5°	0	0	0	0	0
RMS to restraints					
NOE distances (Å)	0.015	0.016	0.013	0.011	0.013
TALOS angles (deg)	0.50	0.42	0.30	0.41	0.26
Deviation from idealized geometry					
Bonds (Å)	0.017	0.019	0.015	0.015	0.014
Angles (°)	1.47	1.51	1.38	1.36	1.26

[a] Atoms C, Cα, O, and N in residue ranges 4–18, 42–53, 60–65, 70–79.

Phosphopantetheine Arrangement and Acyl Chain Binding

The acyl chain conformation is based on a high number of NOE constraints identified in both filtered and ^{13}C-, ^{15}N-edited NOESY experiments. The position of the carbonyl or hydroxyl group of fatty acid part of attachment is dictated by the hydrophobic interaction of the hydrophobic chain with the core ACP

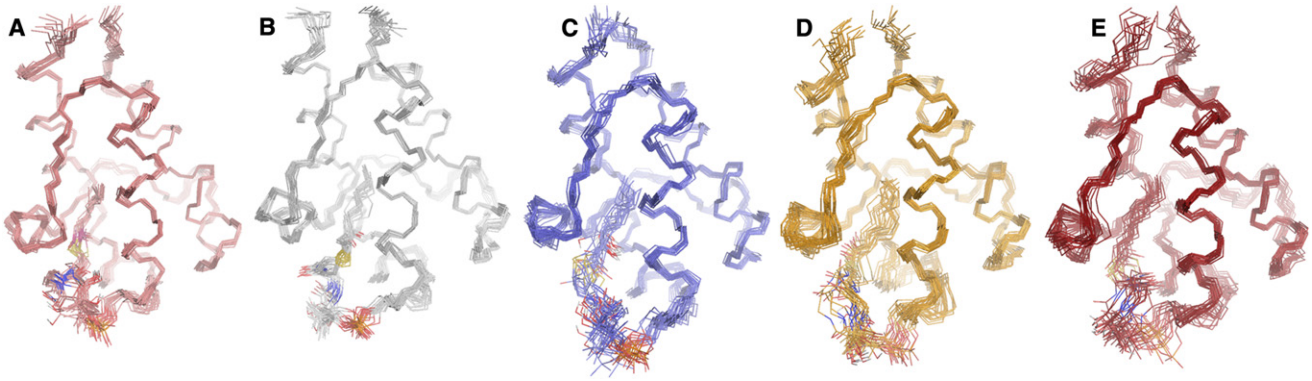

Figure 3. Structural Ensembles for the Best Fit Superposition of the Backbone (N, C^{α}, C) Atoms of the 20 Simulated Annealing Structures
(A) Hexanoyl-ACP (pink), (B) 3-oxooctanyl-ACP (gray), (C) 3*R*-hydroxyoctanoyl-ACP (blue), (D) 2-octenoyl-ACP (yellow), and (E) octanoyl-ACP (red). The protein backbone is presented in lines as well as phosphopantetheine attachment. In all five cases, the superposition was made on the closest to average structure in the ensemble of 20 models over residues 4–18, 42–53, 60–65, and 70–79.

residues (Figure 5). In other words, the position of either carbonyl or hydroxyl group depends on the placement of the acyl part within ACP rather than any specific interactions of these functional groups with the protein. The phosphopantetheine attachment conformation is dictated by NOE contacts between the methylenes and amide protons ($CH_2$37, $CH_2$38, $CH_2$42, $CH_2$43, H_N36, H_N41, see Figure 1B) with hydrophobes placed at the entrance to the cavity (V44, V63, T33, M43). In hexanoyl-ACP, the acyl-4′-PP group is defined by 156 constraints and displays a RMSD of 1.01 Å. The C_1 = O group is positioned near the backbone of K67 with the carbonyl oxygen pointing toward the amide group of F32 (Figure 5A). In 3-oxooctanyl-ACP, the C_3 = O is also immobilized close to the last turn of helix III and faces F32. The

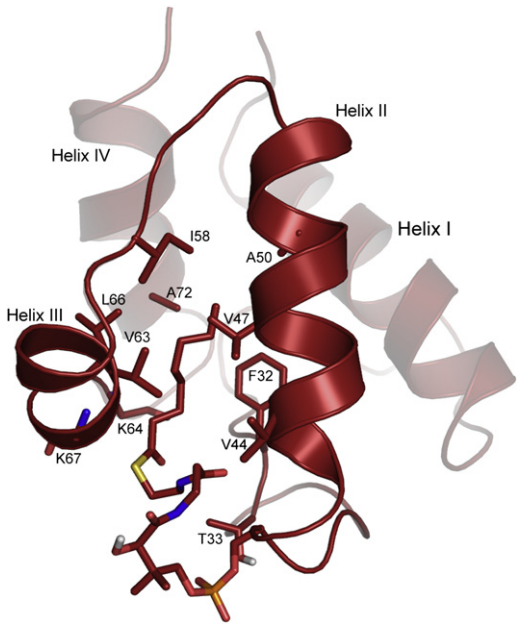

Figure 4. The Hydrophobic Pocket of Octanoyl-ACP
The closest to average structure of octanoyl-ACP (in ribbon, acyl attachment in sticks) with the key residues defining the hydrophobic pocket presented in sticks.

arrangement of the 3-oxooctanyl group is restrained by 144 NOEs and has a RMSD of 0.75 Å (Figure 5B).

For 3*R*-hydroxyoctanoyl-ACP the acyl phosphopantetheine adopts a conformation with a RMSD of 1.83 Å based on 83 NOEs. The 3-hydroxyl group binds adjacent to the backbone of residues L66 and K67 at the end of helix III, in a position similar to the carbonyl position of the previous structures. As a result, although in proximity to helix III, the fatty acid carbonyl group of 3*R*-hydroxyoctanoyl-ACP is pushed away from the protein core and is more disordered than other structures (Figure 5C).

The carbonyl group of the 2-octenoyl-ACP was also observed to pack close to the backbone of K67. The carbonyl oxygen in this species, however, points toward the amide proton of L66 (Figure 5D). The bound fatty acid and 4′-PP arm is defined by 91 protein-ligand NOE contacts and shows an RMSD of 1.10 Å. We were able to assign unambiguously a number of NOE constraints to the double bond hydrogen atoms, arising from contact with the side chains of T33, M43, V47, and V63. Consequently the double bond exhibits a low RMSD of 0.84 Å (C_2, H_{2A}, C_3, H_{3A} atoms, see Figure 1B) and is buried in the protein core in a space close to the backbone of L66 and within a hydrophobic patch created by the side chains of F32, M43, L66, and V63 and the backbone of K64 and K67.

Ninety protein contacts were identified for the octanoyl 4′-PP attachment and the acyl moiety displays a RMSD of 1.20 Å (Figure 5E). In this ACP form, two orientations of the carbonyl group chain are observed (occupied by 10 models each) where the carbonyl oxygen faces either the amide group of F32 (as seen in the hexanoyl-ACP) or the space between helices II and III.

Pair-Wise Comparison of the Three-Dimensional Structures

Given the nature of the function of ACP, one may expect that interaction of the FAS enzymes be determined in some way to increase the efficiency of biosynthesis. It has been suggested that the nature of the covalently attached intermediate induces a specific conformational change in the carrier protein which may help promote the correct protein-protein interactions, and that conformational flexibility induced by the presence or lack of the 4′-PP cofactor on the ACP-related peptidyl carrier protein

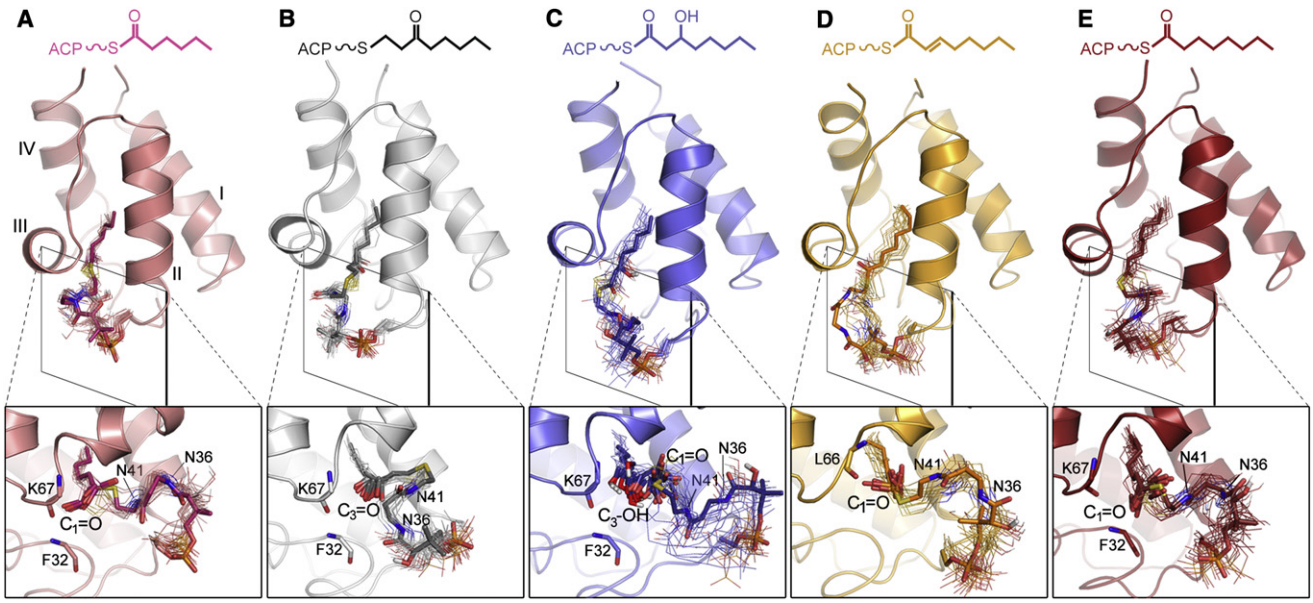

Figure 5. The Overall Folds of Derivatized ACP Forms (top) and Details of the 4′-PP Conformation (bottom)
The closest to average structures are shown in ribbon (protein backbone) and sticks (4′-PP chain). (A) hexanoyl-ACP (pink); (B) 3-oxooctanyl-ACP (gray); (C) 3*R*-hydroxyoctanoyl-ACP (blue); (D) 2-octenoyl-ACP (yellow), and (E) octanoyl-ACP (red). Structures are presented aligned as described in the text.

influences its interactions with other proteins such as the thioesterase and the 4′-PP transferase (Koglin et al., 2006). To study the influence of a given intermediate on ACP conformation, we carried out a pair-wise comparison of ACP forms that interact with the same enzymatic partner (i.e., as reactant and product). In our initial HSQC studies, we identified regions of the protein that adjust to specific intermediates carried by ACP. Pair-wise comparison of the structures confirms that these residues mainly grouped on helix III and at the entrance of the ACP hydrophobic pocket.

The first step in the cycle is condensation of malonyl ACP with a saturated (n)acyl group to produce 3-oxo(n+2)acyl-ACP corresponding to the comparison of hexanoyl-ACP and the 3-oxoacyl mimic, 3-oxooctanyl-ACP. An optimal alignment for these structures is achieved over the backbone atoms (N, O, Cα, C) of helices I, II, and IV (RMSD 0.98 Å). This conversion does, however, induce a significant rearrangement of helix III (RMSD of 2.77 Å) and the phosphopantetheine moiety (Figure 6A). With the C_1 or C_3 carbonyl similarly locked into position next to K67, the hydrophobic tail of the intermediate is buried to the same extent in both forms (Figures 6A and 6B). As a result, the two preceding methylenes (C_1 and C_2) are forced out of the hydrophobic cleft, causing helix III and the 4′-PP moiety to move away from helix II and the sulfur to move closer to helix II. Since both the hexanoyl-ACP C_1 = O group and C_3 = O group of 3-oxooctanyl-ACP bind comparably to the last turn of helix III and the length of the buried hydrophobic chain is identical in both cases, it is likely that the exposure of the two extra carbon atoms is responsible for these rearrangements. This structural feature may play a role in efficient recognition by the ketoreductase.

Following chain elongation, the ketoreductase catalyzes the reduction of the β-keto species (represented by 3-oxooctanyl-ACP) by hydride transfer from NAD(P)H to yield 3*R*-hydroxyacyl-ACP (represented by 3*R*-hydroxyoctanoyl-ACP). The best alignment of the 3-oxooctanyl- with 3*R*-hydroxyoctanoyl-ACP is achieved over the backbone of all four helices, giving a RMSD of 1.05 Å (Figure 6B) with a subtle rearrangement of helix III (RMSD 1.46 Å) and the phosphopantethiene moiety moving away from loop 1 toward helix II. The length of the shielded acyl chain is the same in both cases, and the similarity of the structures suggests that there is little need for additional adjustment to accommodate the hydroxyl group. Moreover, only small changes in helix III occur upon introducing the carbonyl group in position 1 of the acyl chain in 3-hydroxyoctanoyl-ACP. This suggests that when already modified at C_3, the chemical nature of the first carbon (C_1) of the fatty acid may have little influence on the ACP conformation and further supports the idea that the 3-oxooctanyl group is a good mimic of the natural diketoester.

The next step, catalyzed by the dehydratase, involves the elimination of water from 3*R*-hydroxyacyl-ACP (modeled by 3*R*-hydroxyoctanoyl-ACP) to yield 2-enoyl-ACP (represented by 2-octenoyl-ACP). The best alignment of 3-hydroxyoctanoyl-ACP and 2-octenoyl-ACP is achieved over helices I, II, and III (RMSD 0.83 Å) (Figure 6C). Residues 70–75 (part of helix IV) are pushed away from the protein core with a RMSD for the helix IV of 1.69 Å. This change, does not involve any major rearrangement of helices I, III and the majority of helix II and they remain essentially static during this modification. The main displacement is that of helix IV away from helix II. The position of helix IV is similar to that seen for the fully saturated hexanoyl- and octanoyl-ACP. This arises from the carbonyl group (C_1 = O) moving into the position previously occupied by the hydroxyl group (C_3-OH), near helix III and subsequent enlargement of the hydrophobic pocket in order to accommodate the double bond. The conformation of the phosphopantetheine moiety in

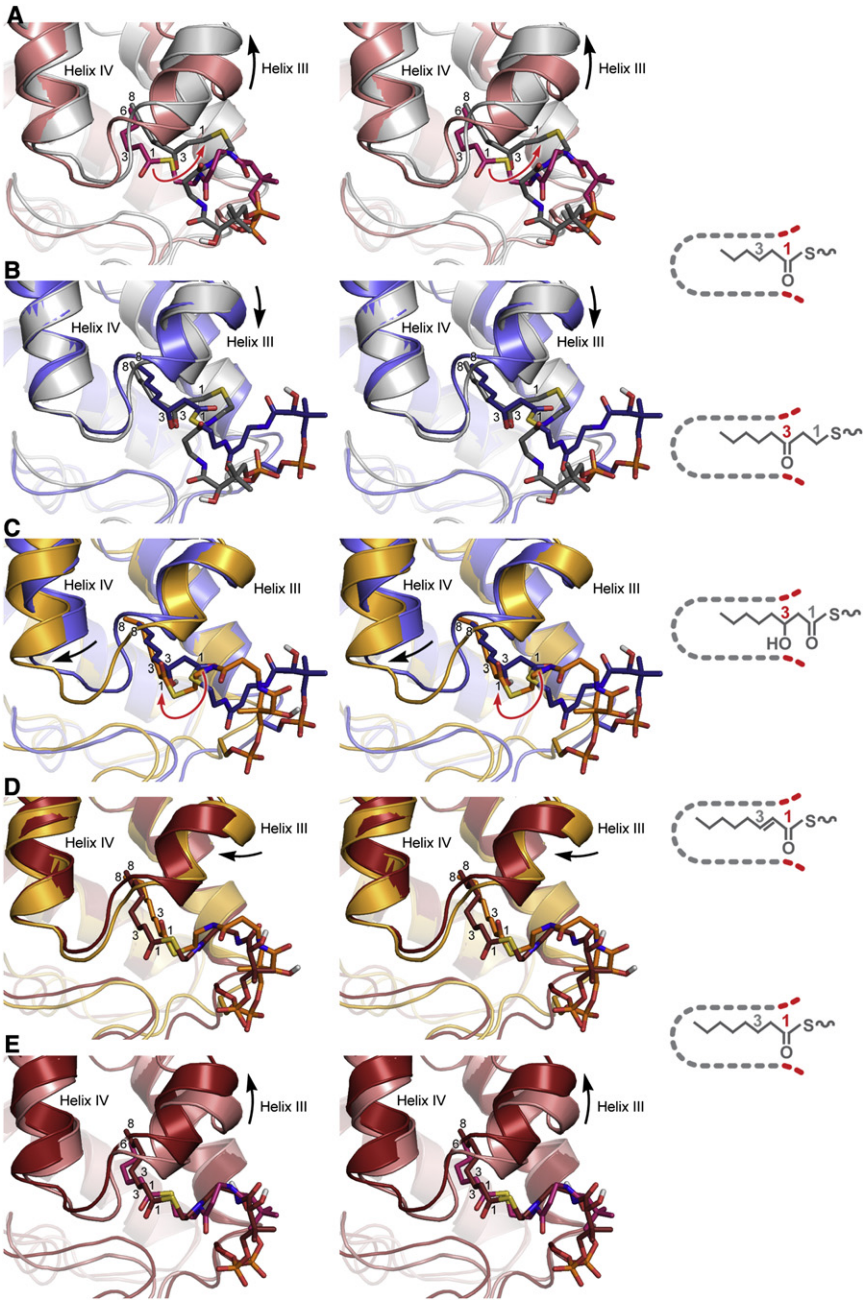

Figure 6. Comparison of the Closest to Average Acyl ACP Structures

The most significant changes are indicated in black (for protein) and red (for 4′-PP) arrows. Stereoviews are shown for (A) hexanoyl- versus 3-oxooctanyl-ACP, (B) 3-oxooctanyl- versus 3*R*-hydroxyoctanoyl-ACP; (C) 3*R*-hydroxyoctanoyl- versus 2-octenoyl-ACP; (D) 2-octenoyl- versus octanoyl-ACP, and (E) hexanoyl- versus octanoyl-ACP. Structures were aligned as described in the text and the color scheme is identical to Figure 6. The right-hand column shows a graphical depiction of the change in chain burial depending on the attached intermediate. The dotted line represents the hydrophobic binding cavity of the fatty acid ACP and the changing position of carbon 1 and carbon 3 is indicated.

2-octenoyl-ACP is also different to 3*R*-hydroxyoctanoyl-ACP and is better defined despite a similar number and distribution of NOE constraints. Surprisingly introduction of the double bond does not cause substantial rearrangement of side chains of helix II or III. It has been suggested that a π-stacking interaction with the conserved phenylalanine (F32) can facilitate recognition of the enoyl-ACP species (Roujeinikova et al., 2007). Our data, however, do not show any specific arrangement of the aromatic ring and double bond in relation to each other.

The final step of the FAS cycle is the enoylreductase catalyzed NAD(P)H-dependent reduction of the *trans*-2-enoyl-ACP species to the fully saturated acyl chain. Aligning the structure of 2-octenoyl-ACP and octanoyl-ACP reveals a movement of helix III (RMSD 1.41 Å) while helices I, II and IV remain essentially static (RMSD 0.91 Å). The fully saturated chain pushes helix III away from helix II, the distance between them increasing by 34% (from 6.4 to 8.6 Å) as measured from the Cα atoms of V44 and D60 (Figure 6D). This enlargement of the pocket is most probably induced by the increased volume (143–149 Å^3) and hydrophobicity (calculated LogP rises from 3.3 to 3.6) of the octanoyl group. The arrangement of the 4′-PP moiety in both structures is similar and both carbonyl groups are immobilized in the same region. Differentiation of these ACPs must therefore be based on another factor, which might be the altered position of helix III.

Finally, comparison of the structures of hexanoyl- and octanoyl-ACP over the full cycle reveals a substantial shift in the position of helix III as the acyl chain is elongated. While the thiol ester carbonyl group is anchored in the identical position adjacent to the last turn of helix III (Figure 6E), the greater volume of the octanoyl versus the hexanoyl side chain causes the hydrophobic cavity to expand considerably. Similar rearrangement has been observed in the structures of acyl-ACP from *S. coelicolor* actinorhodin polyketide synthase, where the repositioning of helix III allows a consistent growth of cavity volume in response to the acyl chain length (Evans et al., 2009). Crystal structures of *E. coli* hexanoyl-, heptanoyl-, and decanoyl-ACP do not show any alteration of protein fold upon binding (Roujeinikova et al., 2007); however, solution NMR structures of the *E. coli* butyryl-ACP, apo, and holo forms display repositioning of the helix III when ACP is acylated (Wu et al., 2009). Comparison of the *S. coelicolor* hexanoyl-ACP with the crystal structure of *E. coli* hexanoyl-ACP shows a difference in

the position of fatty acid carbonyl group. In *E. coli*, ACP the carbonyl group is hidden deeply in the hydrophobic core, while in the *S. coelicolor* hexanoyl-ACP this group is positioned lower, at the entrance to the cavity (Figure 7). Consequently, the arrangement of the phosphopantetheine arm differs between both structures, with the *E. coli* arm adopting a more extended conformation. In the spinach acyl-ACP NMR structures, the termini of both decanoyl and steroyl acyl chains penetrate the ACP core to the same degree suggesting that the terminal end of the acyl chain dictates chain position and expansion of the core is finite (Zornetzer et al., 2006). It may also be possible that the maximum capacity of the core is species specific and related to a preferred cellular fatty acid content. When the maximum capacity of the ACP core is reached, the fatty acid chain is more solvent exposed and can begin to play a role in molecular recognition. It has been shown recently that the length of the acyl chain attached to ACP has a predominant role in ACP induced FabT repressor binding to promoter DNA in *Streptococcus pneumoniae*, supporting this idea (Jerga and Rock, 2009).

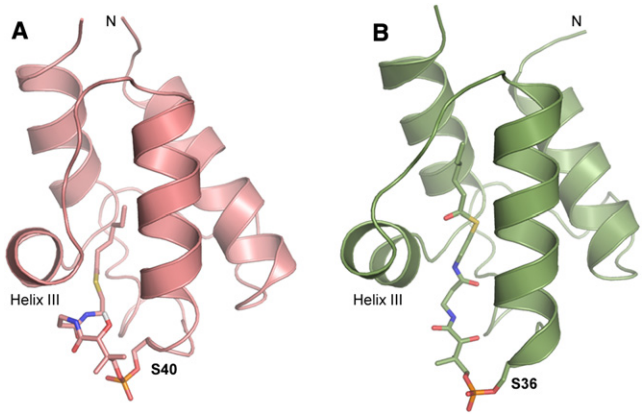

Figure 7. Structural Comparison of acylated *E. coli* and *S. coelicolor* FAS ACPs

Comparison of *E. coli* hexanoyl-ACP (A) structure with *S. coelicolor* (B) hexanoyl-ACP. The protein chain is shown as a ribbon and the acyl-phosphopantetheine is shown in stick representation. Structures have been aligned with one another and presented with helix II toward the reader.

DISCUSSION

Fatty acid biosynthesis depends on efficient delivery of the appropriate substrates to the correct FAS active sites. This is ensured by covalently joining the intermediate with the ACP, as the delivery of the free substrates alone is much less effective (Massengo-Tiassé and Cronan, 2009). Apart from chain elongation, all alterations to the acyl chain occur while the fatty acid intermediate is covalently attached to the ACP, so turnover must involve a combination of molecular recognition (of ACP and FAS partner) and a subsequent mechanism for substrate delivery to each catalytic site.

FAS enzymes position their active sites within long cavities that possess an external docking site for the ACP. Conserved basic residues at the entrance to these tunnels are thought to bind a common recognition motif on helix II of the ACP (Zhang et al., 2003a). Interestingly, helix II remains largely unaltered in each of our studied structures suggesting this important docking site remains preserved despite the changing functionalization of the bound intermediate. This may therefore form common interactions with each of the FAS enzymes irrespective of the nature of the attached intermediate. Over one complete cycle, however, we do observe variations of the intermediate binding and the ACP conformation that on top of this common interaction may modulate interactions with the ketosynthase, ketoreductase, dehydratase, and enoylreductase. ACP binding to its partner enzyme may therefore be driven initially by electrostatic attraction of the two proteins through helix II with conformational changes in the ACP playing little role in this stage (Massengo-Tiassé and Cronan, 2009). Upon binding and formation of the initial assembly, if specific short-range interactions are present, the configuration could then adjust to create a functional complex and the reaction may take place. The conformational changes we have observed, i.e., in the 4′-PP conformation and/or the helix III position, may influence these short-range interactions. If these specific contacts are not satisfied subsequent insertion of the fatty acid chain may not occur unnecessarily, contributing to the overall catalytic efficiency.

A remarkable feature of the ACPs in this study is the consistent locking of the carbonyl or hydroxyl group of the intermediate close to the C terminus of helix III. These structures suggest that over a subsequent elongation cycle, the carbonyl or hydroxyl groups may once again be fixed into the same positions ensuring the ACP always presents a consistent conformation of the 4′-PP sidearm and portion of the fatty acid to an individual FAS enzyme irrespective of fatty acid length. The KR, for example, would be presented with a consistent arrangement of ACP, 4′-PP and 3-oxoacyl portion of the fatty acid chain over many rounds of fatty acid elongation.

Following binding, substrate delivery necessitates moving the first three carbon atoms of the acyl intermediate (C_1, C_2, and C_3) from the carrier protein to within reach of the catalytic residues of the FAS enzyme. This mechanism of substrate delivery to each active site is not well understood, but two simple models for acyl translocation from ACP to the enzyme could be envisaged. First, the acyl chain might be in equilibrium between buried and solvent exposed conformations and from the exposed form the chain inserts into the FAS enzyme. We find no evidence, however, for two-state exchange between bound and unbound forms in any of the ACP structures solved. This is not surprising as the energy required to pull the aliphatic chain from a hydrophobic environment into solvent presents a significant barrier to this process (Chan et al., 2008). Alternatively, binding to the FAS enzyme might trigger chain exposure through extensive conformational changes involving the movement of ACP helices and rearrangement of the partner enzyme. Some support for this comes from the steered molecular dynamics simulations of the delivery pathway of a 3-hydroxydecanoyl group from an ACP core (Colizzi et al., 2008). These studies suggest that helix III undergoes substantial reorganization and loss of the secondary structure as the acyl chain is extruded between helix II and III. Finally, after the reaction is complete, the ACP and modified intermediate are released, and in the cases we have examined each intermediate is rebound by the ACP. It is possible that this enforces a new ACP conformation which triggers dissociation of the complex.

Overall, the mechanism of substrate delivery in bacterial FA production is more complex than the analogous type I synthases where fatty acid intermediates are not sequestered by the ACP (Płoskoń et al., 2008). Through successful evolution, type I mammalian FAS has combined structural and dynamic changes in the linker regions between domains to drive an efficient delivery of the fatty acid intermediate to the correct catalytic site. In type II systems, communication between dissociated FAS enzymes cannot be orchestrated in this way, perhaps necessitating a more central role for the ACP in the biosynthesis. Our data provide the first insights to our knowledge into how ACPs handle oxidized fatty acid intermediates. These structures demonstrate that ACPs are more than mere passive acyl chain carriers and appear capable of subtle information transfer through structural plasticity.

SIGNIFICANCE

Structural analysis of fatty acid synthases is crucial to understanding the mechanistic basis by which fatty acids are made. Central to these synthases is a an acyl carrier protein (ACP) which has been suggested to not only carry intermediates between the various active sites of the synthase, but also to communicate information about the chemical nature of the intermediate to the partner enzyme. This study has focused on the solution phase structures of ACP covalently bound to representatives of each stage in the fatty acid biosynthetic cycle. Our study reveals two key points. First, the carrier protein and the phosphopantetheine chain adopt unique conformations in response to the oxidation level of the intermediate. Second, the general ACP recognition motif on helix II is not changed significantly by acyl chain binding. Consequently, our results suggest that substrate delivery by the ACP is a multistep process. We propose that this proceeds through the formation of an initial complex between the ACP and the enzyme, after which the specific recognition features, induced by acyl chain binding, alter the specificity of binding to either initiate chain delivery or dissociate the ACP-enzyme complex.

EXPERIMENTAL PROCEDURES

Sample Preparation

The expression and purification of isotopically ^{13}C, ^{15}N labeled *S. coelicolor* FAS *apo* ACP has been described previously (Arthur et al., 2009). All synthesized CoAs were purified by HPLC using a Gemini C18 reverse-phase column (100 × 4.6 mm, 5 μm, Phenomenex) using a water-methanol gradient and analyzed by mass spectrometry and collision induced dissociation on a QStar XL QToF instrument (Applied Biosystems). Coenzyme A was purchased from Aldrich. 2-Octenoyl-CoA thioester was synthesized from 85% trans-2-octenoic acid (Aldrich) using the method described previously (Rasmussen et al., 1990). For 3-oxooctanyl-CoA preparation, CoA and oct-1-en-3-one (Aldrich) were used in a 1:1.5 molar ratio, reaction volume was 100 μl, and CoA concentration was 30 μM. The reaction was performed in 25 mM Tris buffer (pH 8.8) containing 50% methanol for 30min in 30°C. 3-Hydroxyacyl-CoA was prepared from S-phenyl 3*R*-hydroxyoctanthioate (synthesis in SI) based on the previously published procedure (Jia et al., 2001).

ACP Modification with ACPS

Apo ACP (100 μM) was modified with ACPS (1 μM) and the corresponding acyl-CoA (500 μM) in Tris buffer (50 mM [pH 8.8]) with $MgCl_2$ (1 mM). Acylation was monitored by electrospray mass spectrometry. All samples were prepared as described by Winston and Fitzgerald (1998) and analyzed in positive ion mode on a QStar XL mass spectrometer (Applied Biosystems).

NMR Experiments

All samples for structure determination were prepared in an identical manner. After conversion to derivatized ACP, protein solution was desalted and buffer was exchanged against phosphate buffer (50 mM in case of hexanoyl-, 3-oxooctanyl-, 2-octenoyl-, octanoyl-ACP and 10 mM for 3-hydroxyoctanoyl-ACP [pH 7.0]) to a final ACP concentration of approximately 1-2 mM. D_2O (5% v/v) was added to this sample and the pH checked. NMR data were collected on either a Varian INOVA (with a room temperature probe) or VNMRS (equipped with a cryoprobe) 600 MHz spectrometer. For ^{15}N, ^{13}C-labeled ACP, ^{1}H-^{15}N sensitivity enhanced HSQC, HNCACB, CBCA(CO)NH, HCCH-TOCSY were acquired for hexanoyl-, 3-oxooctanyl-, 3-octenoyl-, and octanoyl-ACP. ^{13}C,^{15}N dual acquisition (CN) three-dimensional NOESY (Zwahlen et al., 1997) (150 ms) was acquired for all samples. All spectra were processed and viewed with NMRPipe (Delaglio et al., 1995) and CcpN analysis (Vranken et al., 2005). For the acyl chain binding studies, standard sensitivity enhanced ^{1}H-^{15}N HSQC spectra were acquired in Tris buffer (50 mM, pH 7.0). The fatty acid derivatives and the 4′-PP side chains were assigned on basis of double filtered NOESY and TOCSY experiments and [^{1}H-^{12}C]-F_2 → [^{1}H-^{13}C]-F_1 NOEs from a two-dimensional F_2f-NOESY experiment (Breeze, 2000) (400 ms). Protein chemical shifts were assigned on the basis of acquired triple resonance data but also on the basis of comparison of chemical shift values between the forms.

Structure Calculation and Analysis

Structures were calculated using ARIA 1.2 in conjunction with CNS by means of a torsion angle dynamics procedure (Linge et al., 2001), and backbone torsion angle restraints were obtained from chemical shift data using the TALOS algorithm (Cornilescu et al., 1999). Topology and parameter files were modified as described previously (Evans et al., 2009). One hundred structures were calculated in the final run with the 20 lowest energy structures selected and water refined using modified refinement script applied to the RECOORD database (Nederveen et al., 2005). The quality of the structures was assessed by online versions of the programs PROCHECK (Laskowski et al., 1993) (http://deposit.pdb.org/validate) and WHATIF (http://swift.cmbi.ru.nl) (Vriend, 1990). Fitting was performed using the McLachlan algorithm as implemented in the program ProFit (Martin, A.C.R., http://www.bioinf.org.uk/software/profit/) (McLachlan, 1982). The chemical shift perturbation was calculated according to equation: $\Delta\delta_{av} = \{0.5[\Delta\delta\ (^{1}H_N)^2 + (0.2\ \Delta\delta\ (^{15}N))^2]\}^{1/2}$ (Pellecchia et al., 1999).

ACCESSION NUMBERS

The ensemble of 20 NMR structures of each derivatized ACP and associated NMR chemical shifts have been deposited with the Protein Data Bank/Biological Magnetic Resonance Data Bank with the following accession codes: hexanoyl-ACP, 2koo/16524; 3-oxooctanyl-ACP, 2kop/16525; 3*R*-hydroxyctanoyl-ACP, 2koq/16526; 2-octenoyl-ACP, 2kor/16527; octanoyl-ACP, 2kos/16528.

SUPPLEMENTAL INFORMATION

Supplemental Information includes Supplemental Experimental Procedures, two figures, and one table and can be found with this article online at doi:10.1016/j.chembiol.2010.05.024.

ACKNOWLEDGMENTS

This work was supported by the Biotechnology and Biological Sciences Research Council (BB/F014570/1 for P.W.-a.), the Wellcome Trust (WT082352MA for C.W.), and the Engineering and Physical Sciences Research Council (E.P.S.R.C. for A.L.P.K.). We also thank the European Union for a studentship grant to E.P. under the Marie Curie Early Training Award scheme ("BRISENZ").

Received: December 9, 2009
Revised: April 28, 2010
Accepted: May 14, 2010
Published: July 29, 2010

REFERENCES

Arthur, C.J., Szafranska, A.E., Long, J., Mills, J., Cox, R.J., Findlow, S.C., Simpson, T.J., Crump, M.P., and Crosby, J. (2006). The malonyl transferase activity of type II polyketide synthase acyl carrier proteins. Chem. Biol. *13*, 587–596.

Arthur, C.J., Williams, C., Pottage, K., Ploskon, E., Findlow, S.C., Burston, S.G., Simpson, T.J., Crump, M.P., and Crosby, J. (2009). Structure and malonyl CoA-ACP transacylase binding of *Streptomyces coelicolor* fatty acid synthase acyl carrier protein. ACS Chem. Biol. *4*, 625–636.

Breeze, A. (2000). Isotope-filtered NMR methods for the study of biomolecular structure and interactions. Prog. Nucl. Magn. Reson. Spectrosc. *36*, 323–372.

Brignole, E.J., Smith, S., and Asturias, F.J. (2009). Conformational flexibility of metazoan fatty acid synthase enables catalysis. Nat. Struct. Mol. Biol. *16*, 190–197.

Byers, D.M., and Gong, H. (2007). Acyl carrier protein: structure-function relationships in a conserved multifunctional protein family. Biochem. Cell Biol. *85*, 649–662.

Chan, D.I., Stockner, T., Tieleman, D.P., and Vogel, H.J. (2008). Molecular dynamics simulations of the Apo-, Holo-, and acyl-forms of *Escherichia coli* acyl carrier protein. J. Biol. Chem. *283*, 33620–33629.

Colizzi, F., Recanatini, M., and Cavalli, A. (2008). Mechanical features of *Plasmodium falciparum* acyl carrier protein in the delivery of substrates. J. Chem. Inf. Model. *48*, 2289–2293.

Cornilescu, G., Delaglio, F., and Bax, A. (1999). Protein backbone angle restraints from searching a database for chemical shift and sequence homology. J. Biomol. NMR *13*, 289–302.

Cox, R.J., Hitchman, T.S., Byrom, K.J., Findlow, I.S., Tanner, J.A., Crosby, J., and Simpson, T.J. (1997). Post-translational modification of heterologously expressed *Streptomyces* type II polyketide synthase acyl carrier proteins. FEBS Lett. *405*, 267–272.

Delaglio, F., Grzesiek, S., Vuister, G.W., Zhu, G., Pfeifer, J., and Bax, A. (1995). NMRPipe: a multidimensional spectral processing system based on UNIX pipes. J. Biomol. NMR *6*, 277–293.

Evans, S.E., Williams, C., Arthur, C.J., Burston, S.G., Simpson, T.J., Crosby, J., and Crump, M.P. (2008). An ACP structural switch. Conformational differences between the apo and holo forms of the actinorhodin polyketide synthase acyl carrier protein. ChemBioChem *9*, 2424–2432.

Evans, S.E., Williams, C., Arthur, C.J., Ploskon, E., Wattana-Amorn, P., Cox, R.J., Crosby, J., Willis, C.L., Simpson, T.J., and Crump, M.P. (2009). Probing the interactions of early polyketide intermediates with the actinorhodin ACP from *S. coelicolor* A3(2). J. Mol. Biol. *389*, 511–528.

Flaman, A.S., Chen, J.M., Van Iderstine, S.C., and Byers, D.M. (2001). Site-directed mutagenesis of acyl carrier protein (ACP) reveals amino acid residues involved in ACP structure and acyl-ACP synthetase activity. J. Biol. Chem. *276*, 35934–35939.

Jerga, A., and Rock, C.O. (2009). Acyl-acyl carrier protein regulates transcription of fatty acid biosynthetic genes via the FabT repressor in *Streptococcus pneumoniae*. J. Biol. Chem. *284*, 15364–15368.

Jia, Y., Yuan, W., Wodzinska, J., Park, C., Sinskey, A.J., and Stubbe, J. (2001). Mechanistic studies on class I polyhydroxybutyrate (PHB) synthase from *Ralstonia eutropha*: class I and III synthases share a similar catalytic mechanism. Biochemistry *40*, 1011–1019.

Kim, Y., Kovrigin, E.L., and Eletr, Z. (2006). NMR studies of *Escherichia coli* acyl carrier protein: dynamic and structural differences of the apo- and holo-forms. Biochem. Biophys. Res. Commun. *341*, 776–783.

Koglin, A., Mofid, M.R., Löhr, F., Schäfer, B., Rogov, V.V., Blum, M.M., Mittag, T., Marahiel, M.A., Bernhard, F., and Dötsch, V. (2006). Conformational switches modulate protein interactions in peptide antibiotic synthetases. Science *312*, 273–276.

Laskowski, R.A., Moss, D.S., and Thornton, J.M. (1993). Main-chain bond lengths and bond angles in protein structures. J. Mol. Biol. *231*, 1049–1067.

Linge, J.P., O'Donoghue, S.I., and Nilges, M. (2001). Automated assignment of ambiguous nuclear overhauser effects with ARIA. Methods Enzymol. *339*, 71–90.

Massengo-Tiassé, R.P., and Cronan, J.E. (2009). Diversity in enoyl-acyl carrier protein reductases. Cell. Mol. Life Sci. *66*, 1507–1517.

McLachlan, A.D. (1982). Rapid comparison of protein structures. Acta Crystallogr. A *38*, 871–873.

Nederveen, A.J., Doreleijers, J.F., Vranken, W., Miller, Z., Spronk, C.A., Nabuurs, S.B., Güntert, P., Livny, M., Markley, J.L., Nilges, M., et al. (2005). RECOORD: a recalculated coordinate database of 500+ proteins from the PDB using restraints from the BioMagResBank. Proteins *59*, 662–672.

Nilges, M., Macias, M.J., O'Donoghue, S.I., and Oschkinat, H. (1997). Automated NOESY interpretation with ambiguous distance restraints: the refined NMR solution structure of the pleckstrin homology domain from beta-spectrin. J. Mol. Biol. *269*, 408–422.

Pellecchia, M., Sebbel, P., Hermanns, U., Wüthrich, K., and Glockshuber, R. (1999). Pilus chaperone FimC-adhesin FimH interactions mapped by TROSY-NMR. Nat. Struct. Biol. *6*, 336–339.

Peterson, R.D., Theimer, C.A., Wu, H., and Feigon, J. (2004). New applications of 2D filtered/edited NOESY for assignment and structure elucidation of RNA and RNA-protein complexes. J. Biomol. NMR *28*, 59–67.

Płoskoń, E., Arthur, C.J., Evans, S.E., Williams, C., Crosby, J., Simpson, T.J., and Crump, M.P. (2008). A mammalian type I fatty acid synthase acyl carrier protein domain does not sequester acyl chains. J. Biol. Chem. *283*, 518–528.

Rasmussen, J.T., Borchers, T., and Knudsen, J. (1990). Comparison of the binding affinities of acyl-CoA-binding protein and fatty-acid-binding protein for long-chain acyl-CoA esters. Biochem. J. *265*, 849–855.

Roujeinikova, A., Simon, W.J., Gilroy, J., Rice, D.W., Rafferty, J.B., and Slabas, A.R. (2007). Structural studies of fatty acyl-(acyl carrier protein) thioesters reveal a hydrophobic binding cavity that can expand to fit longer substrates. J. Mol. Biol. *365*, 135–145.

Upadhyay, S.K., Misra, A., Srivastava, R., Surolia, N., Surolia, A., and Sundd, M. (2009). Structural insights into the acyl intermediates of the *Plasmodium falciparum* fatty acid synthesis pathway: the mechanism of expansion of the acyl carrier protein core. J. Biol. Chem. *284*, 22390–22400.

Vranken, W.F., Boucher, W., Stevens, T.J., Fogh, R.H., Pajon, A., Llinas, M., Ulrich, E.L., Markley, J.L., Ionides, J., and Laue, E.D. (2005). The CCPN data model for NMR spectroscopy: development of a software pipeline. Proteins *59*, 687–696.

Vriend, G. (1990). WHAT IF: a molecular modeling and drug design program. J. Mol. Graph. *8*, 52–56, 29.

White, S.W., Zheng, J., Zhang, Y.M., and Rock, C.O. (2005). The structural biology of type II fatty acid biosynthesis. Annu. Rev. Biochem. *74*, 791–831.

Winston, R.L., and Fitzgerald, M.C. (1998). Concentration and desalting of protein samples for mass spectrometry analysis. Anal. Biochem. *262*, 83–85.

Wu, B.N., Zhang, Y.M., Rock, C.O., and Zheng, J.J. (2009). Structural modification of acyl carrier protein by butyryl group. Protein Sci. *18*, 240–246.

Zhang, Y.M., Marrakchi, H., White, S.W., and Rock, C.O. (2003a). The application of computational methods to explore the diversity and structure of bacterial fatty acid synthase. J. Lipid Res. *44*, 1–10.

Zhang, Y.M., Wu, B., Zheng, J., and Rock, C.O. (2003b). Key residues responsible for acyl carrier protein and beta-ketoacyl-acyl carrier protein reductase (FabG) interaction. J. Biol. Chem. *278*, 52935–52943.

Zornetzer, G.A., Fox, B.G., and Markley, J.L. (2006). Solution structures of spinach acyl carrier protein with decanoate and stearate. Biochemistry *45*, 5217–5227.

Zwahlen, C., Legault, P., Vincent, S.J.F., Greenblatt, J., Konrat, R., and Kay, L.E. (1997). Methods for measurement of intermolecular NOEs by multinuclear NMR spectroscopy: Application to a bacteriophage lambda N-peptide/*boxB* RNA complex. J. Am. Chem. Soc. *119*, 6711–6721.

